BTS
11–23 May 2026

EURO-LABS Basic Training School

The 3 MV TANDEM accelerator experiment: test case and procedure

IFIN-HH, Bucharest - Măgurele

For NAG (Nuclear Astrophysics Group): D. State, A.Spiridon, L. Trache.

Introduction

Nuclear astrophysics was founded $\sim$ 70 years ago and since then this field of study has matured. Observational astronomy, nuclear physics, cosmo-chemistry, and theoretical astrophysics have all made significant contributions to the modern nuclear astrophysics. New technologies have brought major improvements in the understanding of the origin of the chemical elements from our Universe: powerful computers capable to study the evolution of stars in a multidimensional framework; high energy astrophysics done with space telescopes give new points of view of the Universe; the cosmo-chemistry succeeded to isolate small pieces of stardust found in very old meteorites, this gives a better understanding of the processes occurring in stars but also on how solids are formed (process that occurs due to the fact that matter condenses); and finally the most relevant, for this experiment, the nuclear physics was able to measure reaction cross sections near stellar energies by using facilities that provide either stable or radioactive ion beams but also different measuring setups [1].

Nowadays, the science program of the majority of nuclear physics laboratories already includes Nuclear Astrophysics as a significant component. The experimental studies can be divided into two categories: direct measurements - which study reactions at low energies as they occur in stars or as close to that as possible, followed by extrapolations into the so-called Gamow window - and indirect methods, which use information (such as nuclear data) extracted from reactions at much higher energies to estimate reaction cross sections or reaction rates in the range of energies relevant for astrophysics. This is due to the fact that at low energies the reactions involving charged particles – this is a large part of reactions in stellar environments – are very much hindered by the Coulomb barrier, leading to considerable measurement difficulties. Therefore, the case of direct measurements calls for special experimental solutions. This part of the school presents a facility for direct measurements at low and very low energies typical for nuclear astrophysics. The facility consists of a small and compact tandem accelerator where irradiations are performed and gamma-ray deactivation measurement setups: a β-γ coincidence setup (used to reduce the background) together with an ultra-low background laboratory located in a salt mine where very low radioactivities can be measured. They belong to IFIN-HH and are situated 120 km apart (the salt mine lab. from IFIN-HH location). Their performances are shown using one physics case. This facility is competitive for the study of nuclear reactions induced by alpha particles and by light ions at energies close to or down into the Gamow window [2].

Case study — $^{13}C+^{12}C$

Study Motivation

Most of the important reactions in nucleosynthesis involve nucleons, p - or n - radiative capture. Only few ion-ion reactions are important. The most relevant during the carbon burning phase is the $^{12}C+^{12}C$ fusion reaction. Its complicated resonance structure and the lack of reliable measurements, down into Gamow window, made it difficult to draw clear conclusions. The $^{13}C+^{12}C$ fusion reaction is the ideal case to constrain the $^{12}C+^{12}C$ S-factor. At energies bellow and above the Coulomb barrier, it has been observed that $^{13}C+^{12}C$ and $^{13}C+^{13}C$ cross sections are upper bounds of the $^{12}C+^{12}C$, and match the maxima of the resonance-like structure seen in $^{12}C+^{12}C$, in the range from 10^{-8} to 1 barn (see Fig. 2.1) [3, 4].

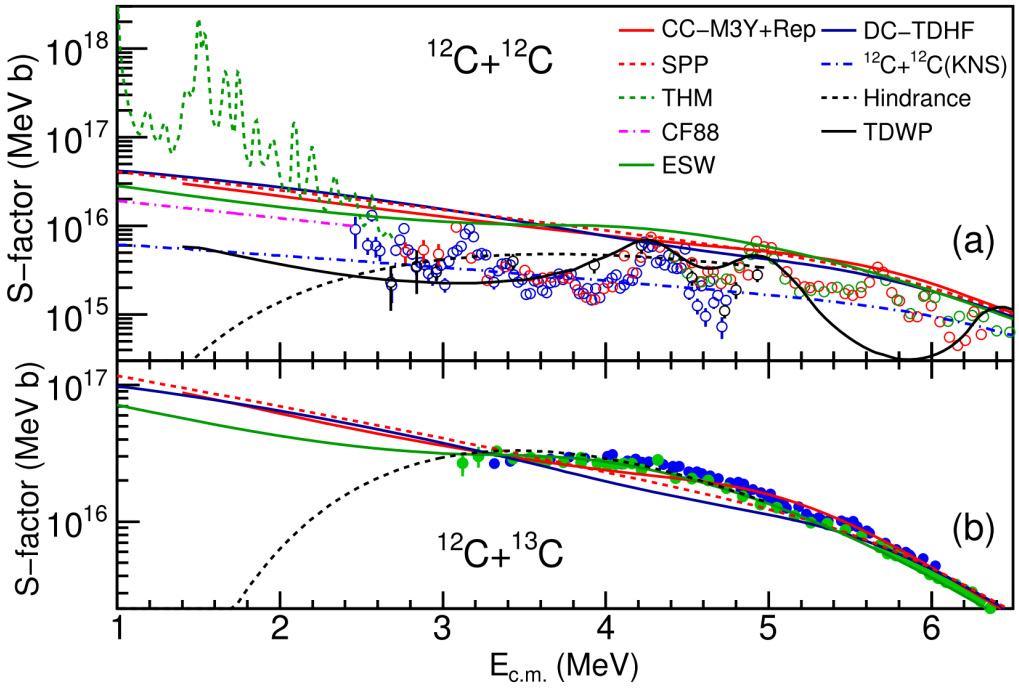

Figure 2.1: The astrophysical S-factors of $^{12}C+^{12}C$ and $^{13}C+^{12}C$ in comparison with model calculations. In panel (a) the $^{12}C+^{12}C$ data with red, green, blue and black empty circles, from [5], [6], [7], [8] are shown. In panel (b), with blue and green full circles, the $^{13}C+^{12}C$ data from [9], [10] are shown [3].

Types of measurements

During the experiment two types of measurements will be performed, prompt gamma ray and de-activation measurements. Excited states of the compound nucleus ^{25}Mg will be populated during the irradiation thus we will detect prompt gamma rays by placing a detector on the accelerator beam line.

$^{12}C + ^{13}C$
(E_{lab} = 10000 keV)

Reaction Products	Q-Value (keV)	Threshold (keV)
^{25}Mg + γ	16317.8	0
^{24}Mg + NN	8987.3	0
^{21}Ne + α	6431.9	0
^{24}Na + p	4253.9	0

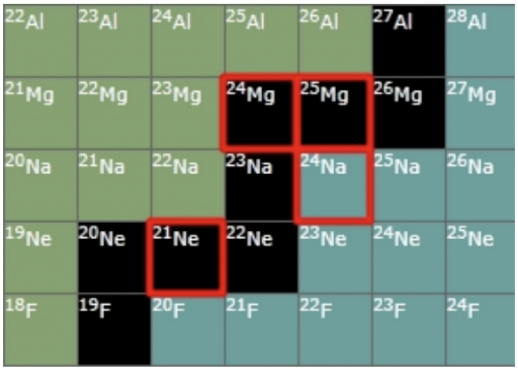

Figure 2.2: Channels opened during the in-beam measurements https://www.nndc.bnl.gov/qcalc/.

The only channel that leads to an unstable nucleus is the proton evaporation channel; it is the only channel for which we can apply the activation method. Its product is ^{24}Na which has a half-life of 14.997 hours [2].

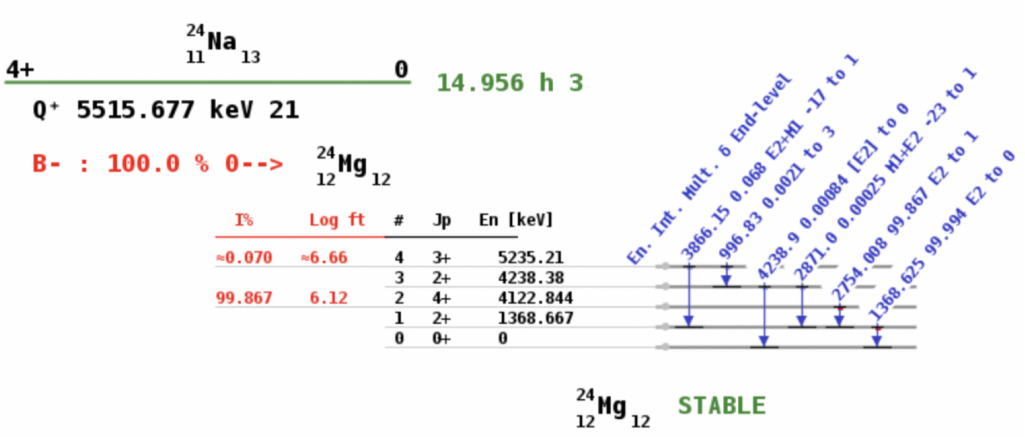

Gamma | CSV | Data API

#	E_γ [keV]	I_γ-(abs) [%]	Initial level [keV]	J^π	Final level [keV]	J^π	Mult.	δ	α_T	I_{Tot} [%]	Comments
1	996.83 *10*	0.0021 *2*	5235.21 *8*	3+	4238.38	2+					
2	1368.625 *5*	**99.994 *2***	1368.667 *5*	2+	0	0+	E2		1.3E-5		
3	2754.008 *11*	99.867 *10*	4122.844 *12*	4+	1368.667	2+	E2				
4	2871.0 *10*	0.00025 *4*	4238.38 *13*	2+	1368.667	2+	M1+E2	-23 *9*			
5	3866.15 *10*	0.068 *6*	5235.21 *8*	3+	1368.667	2+	E2(+M1)	-17 *4*			
6	4238.9 *10*	0.00084 *10*	4238.38 *13*	2+	0	0+	[E2]				

Figure 2.3: Gamma energies together with their probabilities can be found at https://www-nds.iaea.org.

In this experiment ^{13}C beams will hit thick targets of natural carbon (98.93% ^{12}C and 1.07% ^{13}C). The fact that we use a thick target will only affect the way in which the final cross section will be determined.

Experimental procedure

❑ Setup

For **prompt gamma-ray measurements**, a HPGe detector of 100% relative efficiency will be placed at 55^0 with respect to the beam axis in forward direction, at a distance of 13 cm. The final irradiation setup is shown in Fig. 2.4 below. We will determine the contributions from p, n, and α evaporation channels for the energies where reaction cross sections are high enough to be measured [2, 11]. For

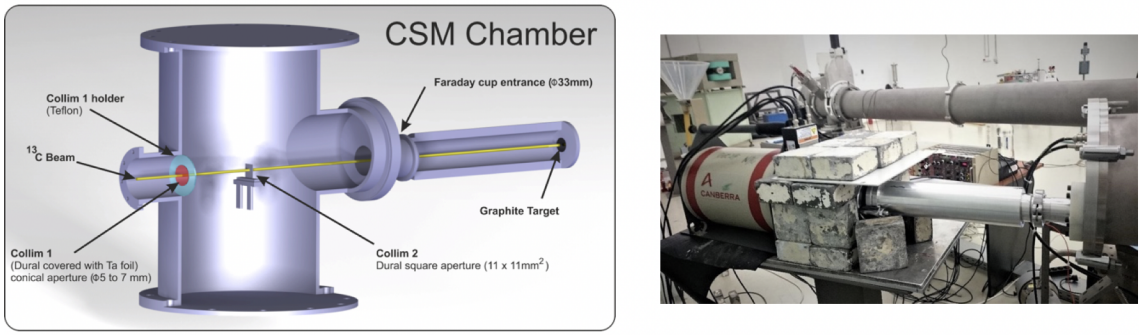

Figure 2.4: Irradiation chamber schematics and the HPGe detector placed inside the lead castle to measure prompt gamma rays [2].

de-activation measurements the irradiated targets will be transported and measured either by using BEGA station (our group lab) or the ultra-low background laboratory, μBq from Slanic Prahova.

BEGA consists of:

- a plastic scintillator with a 20 mm x 20 mm x 2 mm slot in the middle where the activated target will be positioned. It will assure a 4π coverage and therefore, a maximum detection efficiency;
- two HPGe detectors on each side of the target, in closest possible geometry. Space is left for metallic foils (Cu and Sn) to cut low Z X-rays;
- a Pb shield wrapping all 3 detectors.

The β-γ coincidence technique is used to reduce the background that comes from natural decays, such as ^{40}K, natural radon decays, the 511 keV gamma rays from the annihilation of positron-electron and their Compton continuum.

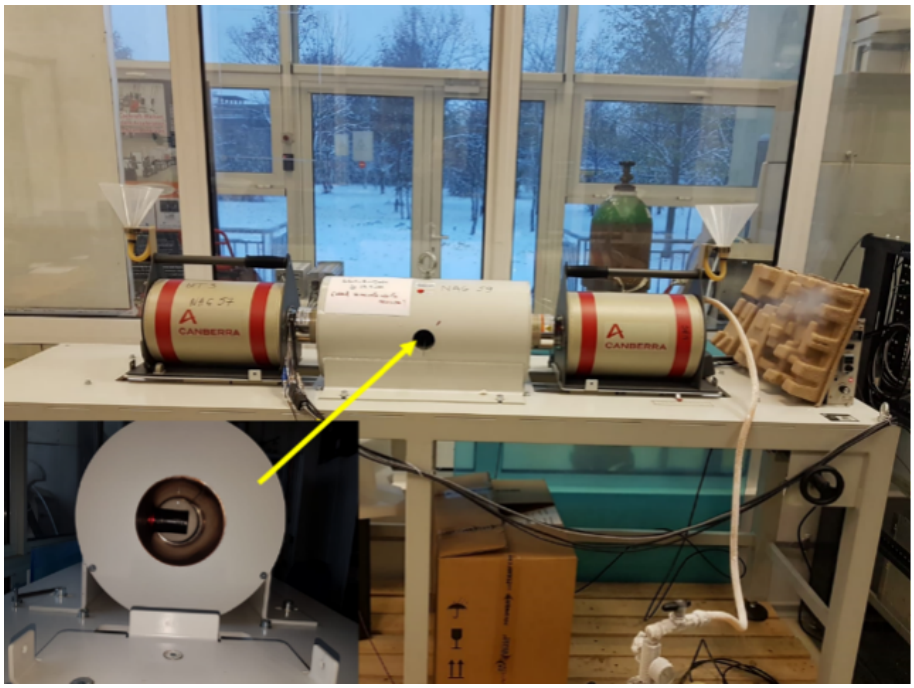

Figure 2.5: The beta-gamma coincidence system [**?**].

The microBequerel (μBq) laboratory of IFIN-HH in Unirea salt mine from Slanic Prahova (located at about 2 hours drive North of Bucharest). The depth of the mine is around 210 m (∼600-meter water equivalent). The reason for which this location has been chosen is the very low natural radioactivity, due to the fact that walls do not present cracks and due to the high purity of the salt. Also, the environmental conditions in the salt mine are very stable year-round: temperature between 12 and 13 ^{0}C, humidity 60-65%. In this mine the laboratory was built to perform measurements using gamma ray spectrometry in ultra-low radiation background. The average dose underground was found to be 1.17 ± 0.14 nGy/h, approximately 80-90 times lower than the dose at the surface [2, 12, 13].

Figure 2.6: The location of the μBq laboratory inside the Slanic salt mine [2, 12]

Figure 2.7 compares natural background γ-ray spectra measured above ground and underground. The top spectrum shows that the strongest components of the γ rays spectrum at E_γ<2.6 MeV are associated with the natural environmental radioactivity and exhibits intense characteristic lines. At higher energies, the background originates mostly from cosmic rays. The natural radioactivity is significantly reduced for measurements in the underground laboratory (bottom spectrum). It can be seen that the measured background radiation (using a protection shield, produced by Canberra Ind., consisting of 15 cm Pb and 5 cm Cu) is about 4000 times smaller compared to the background spectrum measured at the surface. This is the major advantage we want to test and use in the current measurements [2, 12]. The total

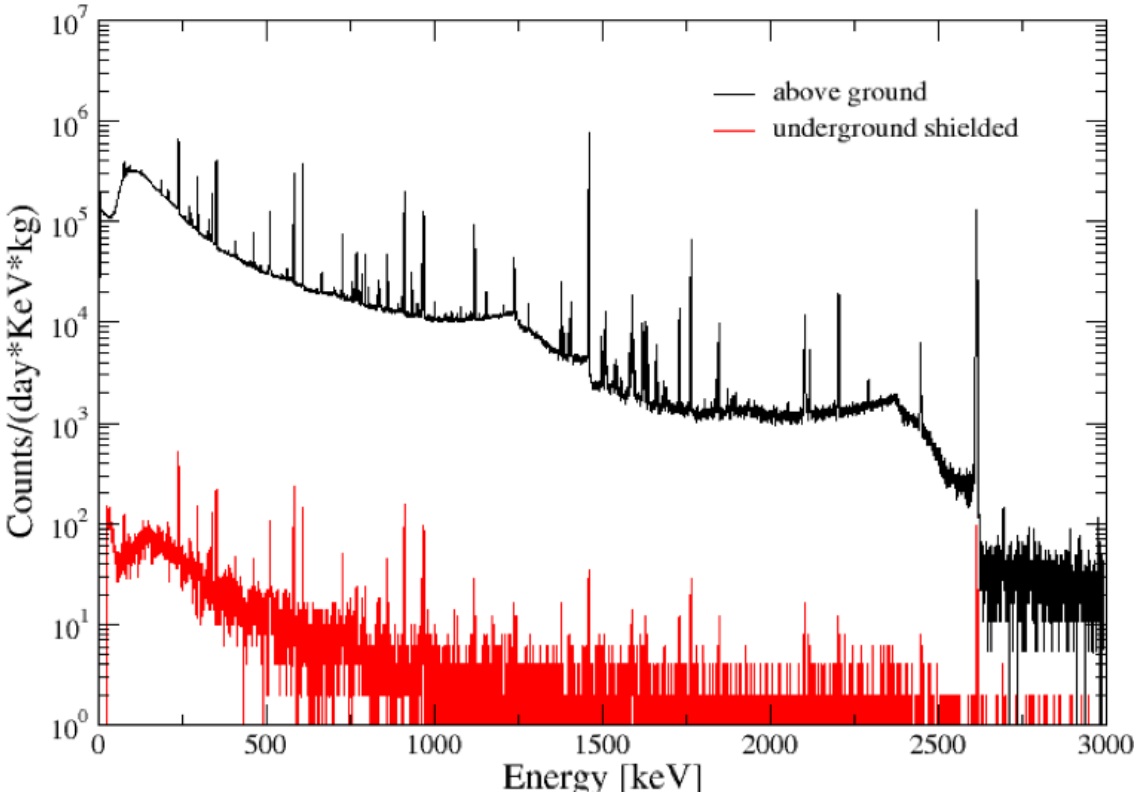

Figure 2.7: Natural background from the μBq laboratory collected with the same HPGe: top is above ground (not shielded), bottom is underground shielded. [2, 12]

counts from 40 to 2700 keV are compared above. The integrated underground rate for this gamma-ray energy region was 25,870 counts in 48 h, that is 539(4) cts/h, (statistical uncertainty only). For comparison we can refer the reader to two underground installations: LUNA at Laboratori Nazionali Gran Sasso [14] and CASPAR at Sanford Underground Research Laboratory in Lead, SD, USA [15]. Both consist of accelerators and detection setups, and are very deep under (3800 mwe- metre water equivalent and 4300 mwe, respectively). Therefore, we can compare only the gamma-ray backgrounds at these places with the one in Slanic, when similar data exist. The underground LUNA facility (accelerator and detectors), under 1.4 km of rock in Gran Sasso, reports [14] a rate of 4870 cts/h in the 1461 keV peak (^{40}K) and 1325 cts/h at the 2614 keV peak (^{232}Th series) with a 137% relative efficiency HPGe detector. Relative efficiency is a common way to express Germanium detec-

tor efficiency. This is the efficiency relative to a ^{60}Co source (using the 1332 keV peak), placed at a distance of 25 cm of from a 3" x 3" NaI(Tl) detector [16]. In a similar detector in Slanic we measure a rate of 1.81 cts/h and 4.8 cts/h in the same peaks. With special shielding, including anti-radon box with dry nitrogen gas flow around the detector, the rates at LUNA become 0.93 cts/h and 0.42 cts/h (setup B in Ref. [14]) for the same two representative gamma-ray background peaks and with extra shielding these rates were reduced by another factor of 2. More recently, at the location of LUNA2 [17] the rates for the same two gamma lines are reported as 2190(10) cts/h and 680(15) cts/h unshielded, and 14.8(3) cts/h and 15.2(3), respectively, for the shielded HPGe detector of 100% relative efficiency (no anti-radon box). At CASPAR, the gamma-ray background in the region 40–2700 keV is essentially the same underground as is at the surface (due to the proximity of rock walls). With shielding the background decreases by a factor 100 in the energy region mentioned [15]. These two latter underground locations are vastly superior in terms of shielding against muons and neutrons, which reflects in reduced background in gamma-ray spectra at E_γ>2.7 MeV [2].

❑ Energy calibration

The object of energy calibration is to derive a relationship between peak position in the spectrum and the corresponding gamma-ray energy. This is normally performed before measurement, if only in a preliminary manner, but it is usual for spectrum analysis programs to include more sophisticated calibration options. Energy calibration is accomplished by measuring the spectrum of a source emitting gamma-rays of precisely known energies and comparing the measured peak position with energy [18]. The energy calibration consists in the experimental determination of a function, usually a first-degree polynomial, describing the energy dependence of the channel number in the spectrum:

$$E_\gamma = A + B \cdot Ch \tag{2.1}$$

where Eγ is the gamma-ray energy, Ch is the spectral channel number for the center of the peak corresponding to Eγ (usually the channel with the maximum number of counts), A and B are constants to be determined for calibration [18]. To do this we will use a ^{152}Eu source.

❑ Detection efficiency calibration

For detection efficiency calibration we will use sources with well-known activities: ^{152}Eu, ^{133}Ba, ^{60}Co, ^{137}Cs. The initial activities of the sources will be provided during the experiment. The present activities can be determined either by hand or using: http://www.radprocalculator.com/Decay.aspx. For **prompt gamma ray measurements**, the radioactive sources will be placed in the same geometry as the targets.

Table 2.1: *Calibration sources initial activities.*

Channel	Λ_0 [Bq] 01.06.2008	Uncertainty [Bq]	$T_{1/2}$
^{152}Eu	389300	±7800	13.517 y
^{133}Ba	34000	± 1020	1925.28 d
^{60}Co	31000	± 900	10.551 y
^{137}Cs	9000	± 270	30.08 y

The most probable gammas used to obtain the efficiency calibration curve, for each source, are listed below:

Table 2.2: *Gamma energies (for each source) used to obtain the efficiency calibration curve.*

Source	E_γ [keV]	I_γ (abs) [%]
^{152}Eu	121.78	28.53
	244.69	7.55
	344.27	26.59
	443.96	2.827
	778.905	12.93
	964.057	14.51
	1112.076	13.67
	1408.013	20.87
^{133}Ba	80.99	32.99
	276.39	7.16
	302.85	18.34
	356.0129	62.05
	383.848	8.94
^{60}Co	1173.228	99.85
	1332.492	99.9826
^{137}Cs	661.657	85.1

We want to have in the end a collective set of measurements, so we will establish notations for every spectrum that we save. For calibration measurements we will name the files as follows: "Isotope[name]_location[on/off]_fargeom.asc" for example: "^{133}Ba_off_fargeom.asc". The next step is to integrate the chosen peaks (coresponding to the listed enrgies in Table 2.2)and obtain the areas (no. of detected counts). We then determine the efficiency as follows:

$$\mathcal{E}_\gamma = \frac{A}{\Lambda \cdot I_\gamma \cdot t_c} \tag{2.2}$$

where:
A is the peak area;
Λ is the source current activity;
I_γ is absolute intensity;
t_c is the counting time.

For de-activation measurements we have to consider the coincidence summing effect.

"The coincidence-summing correction factors, which are important when measuring nuclides decaying through a cascade of successive photon emissions, with high efficiency detectors. The nuclides of the type referred above are quite common; on the contrary, the nuclides without cascade photon emissions are rarely encountered [19]. From the point of view of efficiency of gamma-ray spectrometers, coincidence-summing phenomena led to two fundamental effects:

- coincidence losses from the peak;
- coincidence summing up in the peak.

These effects take place when there is a nonnegligible chance that two or more than two photons originating from the same decay act hit simultaneously the detector [19].

Suppose that one of these photons has deposited completely the energy in the sensitive volume of the detector. In common conditions, a pulse would have been recorded in the full energy peak. But in the case when some additional energy has been deposited in the detector simultaneously by other photons, the pulse is no longer recorded in the full energy peak of the first photon because the energy deposit in the detector is higher than the value corresponding to the peak; that is, count-rate losses from the full energy peak of the first photon are observed. By this phenomenon, the apparent full energy peak efficiency for the given peak of the nuclide in question is smaller than the FEP efficiency at the same energy for a nuclide without cascade photons emission [19].

In other cases, a transition can be produced either directly, by the emission of a single photon with energy E_0, or by the emission of two succesive photons with energies E_1 and E_2:

$$E_0 = E_1 + E_2 \tag{2.3}$$

This is the case eg. of ^{134}Cs, where the 1365 keV photon has exactly the same energy as the sum of the energies of the 569 and 796 keV photons. In such cases, the apparent FEP efficiency for the given nuclide at the energy E_0 is higher than the corresponding efficiency at the energy E_0 for a nuclide without cascade photon emission. Indeed, in the event that the energy of each of the two photons (569 and 796 keV) has been completely absorbed in the detector, the signal corresponding to this event is added to the 1365 keV peak. That is, coincidence summing up increases the apparent FEP efficiency. In certain cases, coincidence summing up is completely responsible for the peak, e.g. the 1785 keV peak of ^{22}Na, which is the result of summing the 1274 keV with the 511 keV produced by positron annihilation, or the 1401 keV peak of ^{134}Cs, which is the result of summing up the 605 and 796 keV photons. Both types of coincidence-summing corrections (coincidence losses and coincidence summing up) depend in a complex way on the decay scheme of the nuclide, on the detector efficiency, on the measurement geometry (including the sample, the detector, the shield), on the sample composition and density [19]."

Experimentally (for de-activation measurements) the coincidence summing correction will be determined by measuring one target placed in close (0 cm) and far

geometry (20 cm). Firstly, we place the radioactive sources at 20 cm from the detector. By doing this we obtain the efficiency of the detector at 20 cm (as in the case of prompt measurements, and by fitting the curve we will obtain $\mathcal{E}_{\gamma 20}$), but we need the efficiency of the detector at 0 cm because this is how we will perform the measurements for our irradiated targets. Secondly, in order to obtain the efficiency of the detector at 0 cm using the efficiency curve for 20 cm we will irradiate one of the targets and perform offline measurements for both 20 cm and 0 cm [2].

For the de-activation measurements, we will determine the detection efficiency for the gamma of interest at 0 cm by using the procedure below. The number of counts detected during the first and the second measurements (at 0 cm and at 20 cm):

$$N_0 = \frac{A \cdot f_{decaymeas} \cdot f_{decaycolling}}{t_m} \tag{2.4}$$

where: A is the area;
t_m is the measurement time.

$$f_{decaymeas.} = \frac{\lambda \cdot t_m}{1 - exp(-\lambda t_m)} \tag{2.5}$$

$$f_{decaycolling} = exp(\lambda \Delta t) \tag{2.6}$$

where Δ t=t_{m0}-t_{m20} and at 0 cm Δt=0. Similar we determine N_{20}.
The last step is the detection efficiency at 0 cm (for the gamma of interest) determined as:

$$\mathcal{E}_{\gamma 0} = \frac{N_0}{N_{20}} \cdot \mathcal{E}_{\gamma 20} \tag{2.7}$$

❑ Cross section determination for de-activation meas.

In an offline spectrum (de-activation measurements) we will see gammas coming from ^{24}Na decaying into ^{24}Mg. The gamma energies and probabilities are:

Table 2.3: *^{24}Na gamma energies and probabilities.*

E_γ [keV]	I_γ (abs) [%]
1368.626	99.9936
2754.007	99.855

The cross section for ^{24}Na was extracted starting from the thick target yield:

$$Y(E) = \int_0^E \frac{dx}{dE} \frac{N_A}{A_t} dE \tag{2.8}$$

where:
$\frac{dx}{dE} = Range\ (g/cm^2)$ determined using LISE++.

➢ **Firstly, we have to calculate the activity at the end of irradiation (for each target) as follows:**

For the deactivation measurements, the first step was to calculate the activity of the target material at the end of irradiation. This was reconstructed using offline γ-counting data to account for decay occurring during the waiting period and the measurement itself:

$$N_{irr} = \frac{R}{\lambda}(1 - e^{-\lambda t_{irr}}) \tag{2.9}$$

where λ is the decay constant of the product nucleus, t_{irr} is the irradiation time and R is the nuclear reaction rate.

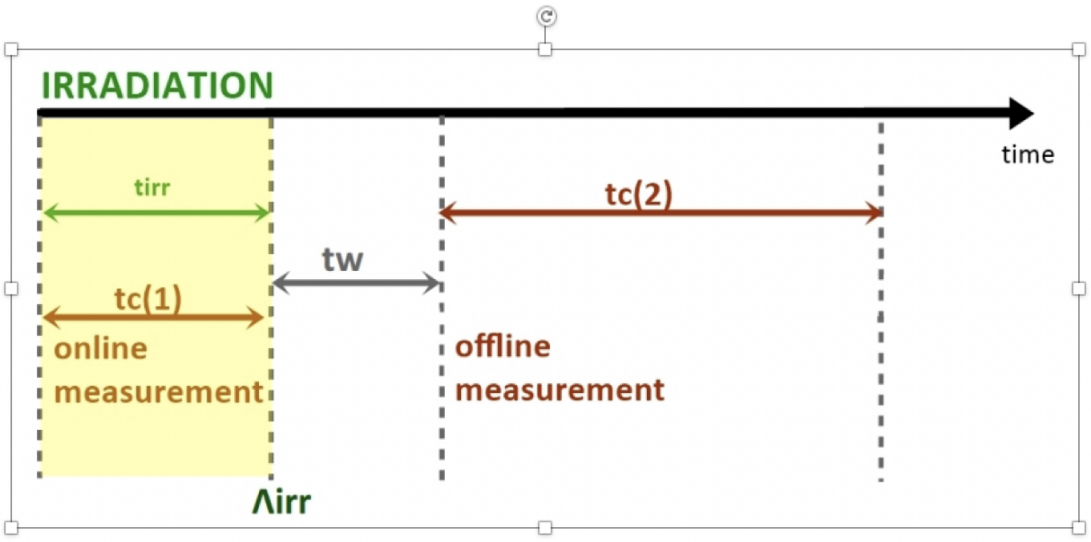

Figure 2.8: De-activation measurements procedure.

➢ **Secondly the thick target yield:**

We defined the yield Y_{decay} as:

$$Y_{decay} = \frac{N_{irr}}{N_p} \tag{2.10}$$

Based on the preceding equations the yield is given by:

$$Y_{decay}(E) = \frac{\lambda N_\gamma e^{\lambda t_w}}{(1 - e^{-\lambda t_c})(1 - e^{-\lambda t_{irr}}) I_\gamma \varepsilon_\gamma} \cdot \frac{1}{N_p} \tag{2.11}$$

where t_w is the waiting time between the end of irradiation and the start of counting and t_c is the counting time.

➢ **The last step is the cross-section determination:**

For a thick target we have to consider that the beam of ^{13}C penetrates to different depths for different energies:

$$\sigma(E) = \frac{Y(E) - Y(E - \Delta E)}{n_t} \tag{2.12}$$

where:
ΔE= 0.2 MeV [in laboratory frame]; n_t is the surface density of nuclei in Δx [nuclei/cm^2].

$$n_t = \rho \frac{N_A}{A} \Delta x \tag{2.13}$$

ρ=2.253 [g/cm^3] (for carbon target);
N_A - Avogadro's number;
A - mass number 12,011 g/mole.

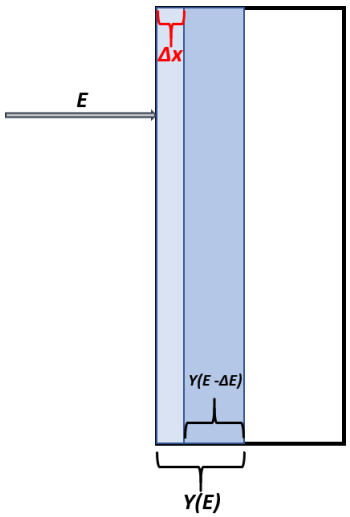

Figure 2.9: Schematic description of the thick target method [2].

The range x for each energy can be obtained using LISE++ (*https : //lise.nscl.msu.edu/porting/download_utilites.html*, Δx=x_2-x_1. Finally we can determine the cross section corresponding to an effective energy E_1<E_{eff}<E_2. In this case the cross section corresponds to an effective energy,E_{eff}, which is a point between E and E-ΔE and where the area under the cross section curve is divided equally between E-ΔE to E_{eff} and E_{eff} to E [20].The effective energy will be determined as follows [20]:

$$E_{eff} \approx (E - \Delta E) + \Delta E \left(\frac{ln\left(1/2 + Y(E)/2Y(E - \Delta E)\right)}{ln\left(Y(E)/Y(E - \Delta E)\right)} \right) \tag{2.14}$$

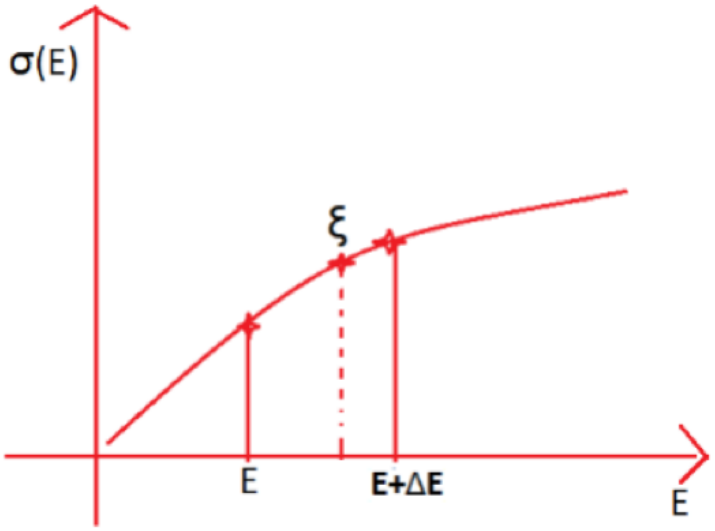

Figure 2.10: Effective energy.

❑ Cross section determination for prompt meas.

The determination of the cross section is similar with that from de-activation measurements. Data analysis starts with:

➢ **time integration of the beam current in order to obtain the total charge which hits the targets to determine the number of projectiles:**

$$N_p = \frac{Q(C)}{e \cdot q} \tag{2.15}$$

where Q(C)= I·Δt - is the total charge. Then the reaction channel yield is:

$$Y_{ch}(E) = \frac{N_\gamma}{\varepsilon_\gamma N_p} \tag{2.16}$$

where ε_γ is the photo-peak efficiency. The gamma energies and probabilities:

Table 2.4: *The channels that open during the irradiation [11].*

Channel	E_γ [keV]
^{21}Ne+α	350.7
^{24}Na+p	472.2
^{24}Mg+n	1368.63

The 3 MV Tandem Accelerator

❑ Accelerator's performance and calibration.

A TANDEM is a two-stage accelerator and its working principle is based on direct acceleration in an electrostatic field, created by the high voltage terminal, together with a system which doubles the energy. The TANDEM accelerator terminal is charged with positive voltage and has two acceleration columns, one toward each side of the terminal. The ion source, which is placed outside of the acceleration system, produces a negative ion beam that is firstly accelerated toward the terminal. The energy gain in this first stage is:

$$E_I = e \cdot U \tag{2.17}$$

As the beam reaches the terminal, the negative ions are stripped by a thin foil or a gas to form positive ions, which are then accelerated away in the second column. The energy gained in this stage is:

$$E_{II} = e \cdot q \cdot U \tag{2.18}$$

where:
q - is the charge state;
e - is the elementary charge=1.6 $\cdot 10^{-19}$C.
The final beam energy, in MeV, is:

$$E = (q + 1) \cdot U \tag{2.19}$$

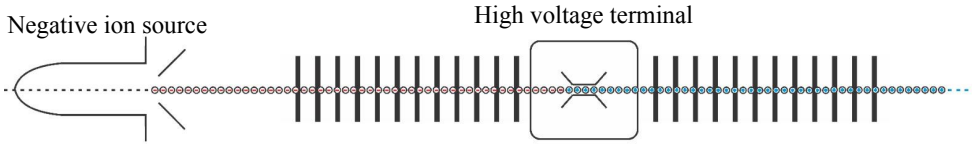

Figure 2.11: Two-stage TANDEM accelerator [21].

The 3 MV Tandetron^{TM} was designed and built by High Voltage Engineering Europa B.V. and commissioned at IFIN-HH in 2012. Its original intended use was Ion Beam Analysis (IBA) with various methods: Rutherford BackScattering (RBS), Elastic Recoil Detection Analysis (ERDA), Particle Induced X-rays Emission (PIXE), Particle Induced Gamma-rays Emission (PIGE), Nuclear Reaction Analyses (NRA) and ion implantation, as described in Ref. [22]. The layout of the Tandetron^{TM} and its beam lines are shown in Fig. 2.12 [2].

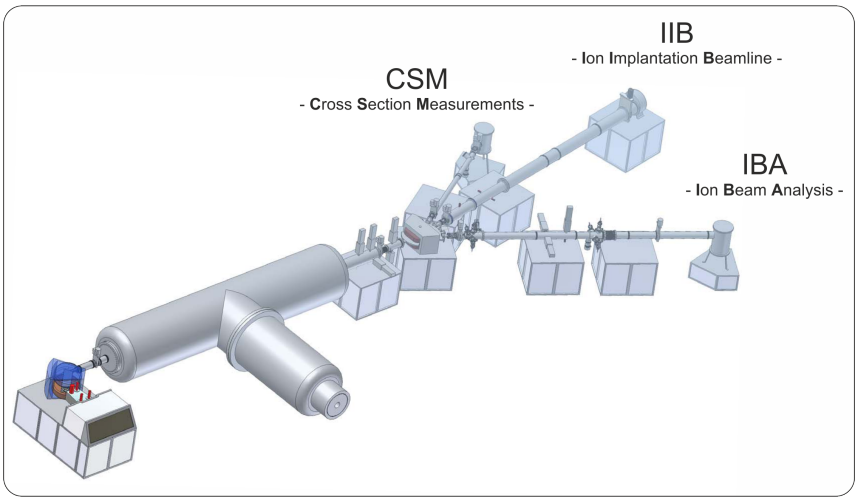

Figure 2.12: Outline of the 3MV [2].

Accelerator's calibration

In Nuclear Astrophysics (NA) a good knowledge of beam energies is very important. Therefore, we have to calibrate the tandem. The accelerator high voltage is monitored by a generating voltmeter (GVM) that provides feedback for the Tandetron^{TM} driver. GVM requires periodic calibration and for this work the resonant reaction ^{27}Al(p,γ)^{28}Si will be used [23, 24]. The well-known narrow resonance

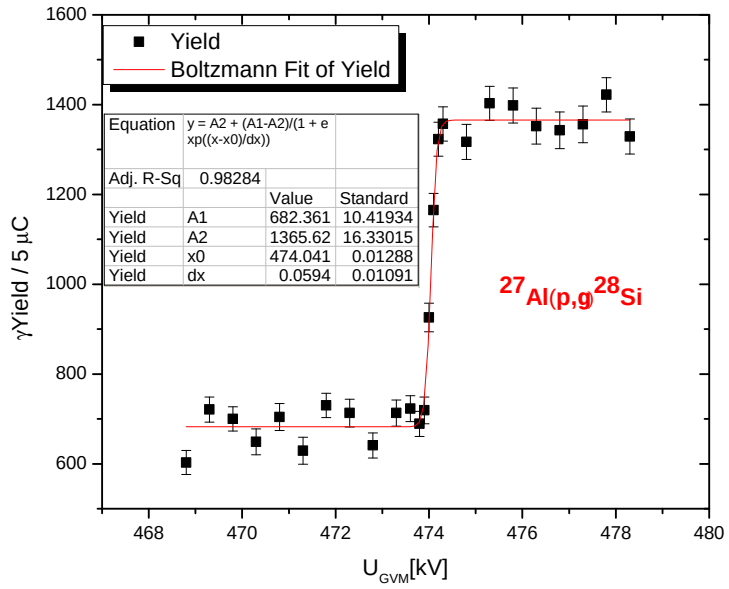

Figure 2.13: Excitation function for the ^{27}Al(p,γ)^{28}Si at 992 keV resonance.

at E$_p$=992 keV will be scanned in 0.1 kV steps and the excitation will be obtained (see Figure 2.13). In order to determine the calibration curve (Figure 2.14) two more cross-section maxima will be measured near 1317 keV, respectively 1381 keV [25]. In previous experiment, the three points allowed for the determination of the intercept 0.9495 and a 0.9930(5) kV slope in Fig. 2.14 bottom. We estimated the uncertainty on E to be less than 0.1% [2].

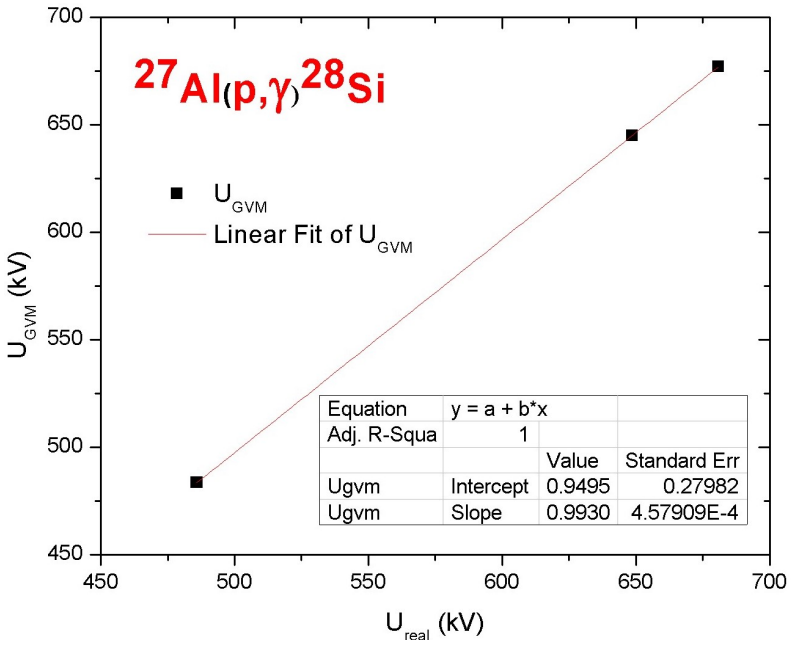

Figure 2.14: The 3 MV Tandetron^{TM} GVM calibration curve [2].

Irradiation plan

The machine has a maximum voltage of 3 MV, and it can run as low as 200 kV. For our experiment we will use ^{13}C beams, double or triple ionized (q=2^+ or q=3^+, depending on energy). The beam current will vary with the energy, at higher energies we will use lower currents as the cross section is high enough. At lower energies, the beam current will be higher because the cross sections decrease significantly. Also, the irradiation time will depend on energy.

Table 2.5: *Irradiation plan.*

Target	E_{beam} [MeV]	Charge state	beam current aprox. [μA]	t_{irr}	Comments
T_1	8	3^+	8	1.5	BEGA+Online meas.
T_2	8.2	3^+	7	1.5	BEGA+Online meas.
T_3	8.4	3^+	7	1.5	BEGA+Online meas.
T_4	8.6	3^+	6	1	BEGA+Online meas.
T_5	8.8	3^+	6	1	BEGA+Online meas.
T_6	9	3^+	5	1	BEGA+Online meas.
T_7	6.6	2^+	10	3	BEGA+μBq

Bibliography

[1] J. José, C. Iliadis, Nuclear astrophysics: the unfinished quest for the origin of the elements Rep. Prog. Phys. 74 (2011) 096901.

[2] D. Tudor, L. Trache, A. Chilug, I. Stefanescu, A. Spiridon, M. Straticiuc, I. Burducea, A. Pantelica, R. Margineanu, D. Ghita, D. Pacesila, R. Andrei, C. Gomoiu, N. Zhang, X. Tang, A facility for direct measurements for nuclear astrophysics at IFIN-HH - a 3 MV tandem accelerator and an ultra-low background laboratory Nucl. Instrum. Methods Phys. Res. A 953 (2020) 163178 .

[3] N. Zhang, X. Wang, D. Tudor, B. Bucher, I. Burducea, H. Chen, Z. Chen, D. Chesneanu, A. Chilug, L. Gasques, D. Ghita, C. Gomoiu, K. Hagino, S. Kubono, Y. Li, C. Lin, W. Lin, R. Margineanu, A. Pantelica, I. Stefanescu, M. Straticiuc, X. Tang, L. Trache, A. Umar, W. Xin, S. Xu, Y. Xu, Constraining the ^{12}C+^{12}C astrophysical S-factors with the ^{12}C+^{13}C measurements at very low energies, Phys. Lett. B 801 (2020) 135170.

[4] M. Notani, H. Esbensen, X. Fang, B. Bucher, P. Davies, C. L. Jiang, L. Lamm, C. J. Lin, C. Ma, E. Martin, K. E. Rehm, W. P. Tan, S. Thomas, X. D. Tang, E. Brown, Correlation between the ^{12}C+^{12}C, ^{12}C+^{13}C, and ^{13}C+^{13}C fusion cross sections Phys. Rev. C 85 (2012) 014607.

[5] H. W. Becker, K. U. Kettner, C. Rolfs, H. P. Trautvetter, The $^{12}\mathbf{C}$ +^{12} **C** reaction at subcoulomb energies (II) Zeitschrift für Physik A Atoms and Nuclei 303 (1981) 305-312.

[6] E. F. Aguilera, P. Rosales, E. Martinez-Quiroz, G. Murillo, M. Fernández, H. Berdejo, D. Lizcano, A. Gómez-Camacho, R. Policroniades, A. Varela, E. Moreno, E. Chávez, M. E. Ortíz, A. Huerta, T. Belyaeva, M. Wiescher, New γ-ray measurements for ^{12}C +^{12}C sub-coulomb fusion: Toward data unification Phys. Rev. C 73 (2006) 064601.

[7] T. Spillane, F. Raiola, C. Rolfs, D. Schürmann, F. Strieder, S. Zeng, H.-W. Becker, C. Bordeanu, L. Gialanella, M. Romano, J. Schweitzer, ^{12}C+^{12}C fusion reactions near the gamow energy Phys. Rev. Lett. 98 (2007) 122501.

[8] C. L. Jiang, D. Santiago-Gonzalez, S. Almaraz-Calderon, K. E. Rehm, B. B. Back, K. Auranen, M. L. Avila, A. D. Ayangeakaa, S. Bottoni, M. P. Carpenter, C. Dickerson, B. DiGiovine, J. P. Greene, C. R. Hoffman, R. V. F. Janssens, B. P. Kay, S. A. Kuvin, T. Lauritsen, R. C. Pardo, J. Sethi, D. Seweryniak, R. Talwar, C. Ugalde, S. Zhu, D. Bourgin, S. Courtin, F. Haas, M. Heine,

G. Fruet, D. Montanari, D. G. Jenkins, L. Morris, A. Lefebvre-Schuhl, M. Alcorta, X. Fang, X. D. Tang, B. Bucher, C. M. Deibel, S. T. Marley, Reaction rate for carbon burning in massive stars Phys. Rev. C 97 (2018) 012801.

[9] R. Dayras, R. Stokstad, Z. Switkowski, R. Wieland, Gamma-ray yields from ^{12}C+ ^{13}C reactions near and below the coulomb barrier Nuclear Physics A 265 (1976) 153-188.

[10] B. Dasmahapatra, B. Čujec, F. Lahlou, Fusion cross sections for ^{12}C+ ^{12}C , ^{12}C+ ^{13}C and ^{13}C+ ^{13}C at low energies Nuclear Physics A 384 (1982) 257-272.

[11] A. I. Chilug, D. Tudor, L. Trache, M. Straticiuc, I. Burducea, I. Focsa, D. G. Ghită, N. T. Zhang, X. Tang, H. Chen, Experiments in IFIN-HH to determine reaction cross sections for the ^{13}C+^{12}C system through direct measurements at very low energies, Presentation at 17th Russbach School on Nuclear Astrophysics.

[12] R. Margineanu, C. Simion, S. Bercea, O. Duliu, D. Gheorghiu, A. Stochioiu, M. Matei, The Slanic-Prahova (ROMANIA) underground low-background radiation laboratory Appl. Radiat. Isot. 66 (2008) 1501-1506.

[13] B. Mitrica, R. Margineanu, S. Stoica, M. Petcu, I. M. Brancus, A. Jipa, I. Lazanu, O. Sima, A. Haungs, H. Rebel, M. Petre, G. Toma, A. Saftoiu, A. Apostu, Estimation of m.w.e (meter water equivalent) depth of the salt mine of Slanic Prahova, Romania, AIP Conf. Proc. 1304 (2010) 331-335.

[14] A. Caciolli, L. Agostino, D. Bemmerer, R. Bonetti, C. Broggini, F. Confortola, P. Corvisiero, H. Costantini, Z. Elekes, A. Formicola, Z. Fülöp, G. Gervino, A. Guglielmetti, C. Gustavino, G. Gyürky, G. Imbriani, M. Junker, M. Laubenstein, A. Lemut, B. Limata, M. Marta, C. Mazzocchi, R. Menegazzo, P. Prati, V. Roca, C. Rolfs, C. Rossi Alvarez, E. Somorjai, O. Straniero, F. Strieder, F. Terrasi, H. P. Trautvetter, T. L. Collaboration, Ultra-sensitive in-beam γ-ray spectroscopy for nuclear astrophysics at LUNA The Eur. Phys. J. A 39 (2009) 179-186.

[15] Robertson, Daniel, Couder, Manoel, Greife, Uwe, Strieder, Frank, Wiescher, Michael, Underground nuclear astrophysics studies with CASPAR EPJ Web of Conferences 109 (2016) 09002.

[16] Mirion technologies:https://www.mirion.com/learning-center/lab-experiments/gamma-ray-efficiency-calibration-lab-experiment.

[17] A. Boeltzig, A. Best, G. Imbriani, M. Junker, M. Aliotta, D. Bemmerer, C. Broggini, C. G. Bruno, R. Buompane, A. Caciolli, F. Cavanna, T. Chillery, G. F. Ciani, P. Corvisiero, L. Csedreki, T. Davinson, R. J. deBoer, R. Depalo, A. D. Leva, Z. Elekes, F. Ferraro, E. M. Fiore, A. Formicola, Z. Fülöp, G. Gervino, A. Guglielmetti, C. Gustavino, G. Gyürky, I. Kochanek, R. Menegazzo, V. Mossa, F. R. Pantaleo, V. Paticchio, R. Perrino, D. Piatti, P. Prati, L. Schiavulli, K. Stöckel, O. Straniero, F. Strieder, T. Szücs, M. P.

Takács, D. Trezzi, M. Wiescher, S. Zavatarelli, Improved background suppression for radiative capture reactions at LUNA with HPGe and BGO detectors J. Phys. G: Nucl. and Par. Phys. 45 (2018) 025203.

[18] G. Gilmore, Practical Gamma-ray Spectrometry, John Wiley Ltd, The Atrium, Southern Gate, Chichester, 2008.

[19] O. Sima, D. Arnold, C. Dovlete, Gespecor: A versatile tool in gamma-ray spectrometry J. Radioanal. Nucl. Chem. 248 (2001) 359-364.

[20] J. Zickefoose, $^{12}C+$ ^{12}C Fusion: Measurement and Advances Toward the Gamow Energy PhD Thesis, University of Connecticut, 2011.

[21] R. Van De Graaff, Tandem electrostatic accelerators Nucl. Instrum. and Methods 8 (1960) 195-202.

[22] I. Burducea, M. Straticiuc, D. G. Ghită, D. V. Moşu, C. I. Călinescu, N. C. Podaru, D. J. W. Mous, I. Ursu, N. V. Zamfir, A new ion beam facility based on a 3 MV Tandetron^{TM} at IFIN-HH, Romania Nucl. Instrum. Methods Phys. Res. Sect. B 359 (2015) 12-19.

[23] P. Kirkpatrick, I. Miyake, a Generating Voltmeter for the Measurement of High Potentials Rev. Sci. Instrum. 3 (1932) 1-8.

[24] J. B. Marion, Accelerator Calibration Energies Rev. Mod. Phys. 34 (1966) 660-668.

[25] C. Chronidou, K. Spyrou, S. Harissopulos, S. Kossionides, T. Paradellis, Resonance strength measurements of the ^{27}Al(p,γ)^{28}Si reaction in the energy range E_p= 0.8–2.0 MeV Eur. Phys. J. A 6 (1999) 303-308.